



OPEN ACCESS

Microscopic return point memory in Co/Pd multilayer films

To cite this article: K A Seu *et al* 2010 *New J. Phys.* **12** 035009

View the [article online](#) for updates and enhancements.

You may also like

- [Comprehensive analysis of electrothermally driven nanoscale insulator–metal transition SmNiO₃-based selector for cross-point memory array](#)
Saiful Haque Misha, Nusrat Tamanna, Amit Prakash et al.
- [Focus on X-ray Beams with High Coherence](#)
Ian Robinson, Gerhard Gruebel and Simon Mochrie
- [A C–Te-based binary OTS device exhibiting excellent performance and high thermal stability for selector application](#)
Solomon Amsalu Chekol, Jongmyung Yoo, Jaehyuk Park et al.

Microscopic return point memory in Co/Pd multilayer films

K A Seu^{1,2}, R Su¹, S Roy², D Parks¹, E Shipton³, E E Fullerton³ and S D Kevan¹

¹ Physics Department, University of Oregon, Eugene, OR 97403, USA

² Advanced Light Source, Lawrence Berkeley National Laboratory, Berkeley, CA 94720, USA

³ Electrical and Computer Engineering, University of California, San Diego, CA 92093, USA

E-mail: sroy@lbl.gov

New Journal of Physics **12** (2010) 035009 (15pp)


Received 2 October 2009

Published 31 March 2010

Online at <http://www.njp.org/>

doi:10.1088/1367-2630/12/3/035009

Abstract. We report soft x-ray speckle metrology measurements of microscopic return point and complementary point memory in Co/Pd magnetic films having perpendicular anisotropy. We observe that the domains assemble into a common labyrinth phase with a period that varies by nearly a factor of two between initial reversal and fields near saturation. Unlike previous studies of similar systems, the ability of the film to reproduce its domain structure after magnetic cycling through saturation varies from loop to loop, from position to position on the sample, and with the part of the speckle pattern used in the metrology measurements. We report the distribution of memory as a function of field and discuss these results in terms of the reversal process.

 Online supplementary data available from stacks.iop.org/NJP/12/035009/mmedia

Contents

1. Introduction	2
2. Experimental procedures	3
3. Results and discussion	5
3.1. Scattering envelope and average domain structure	5
3.2. Microscopic memory measurements	7
3.3. Stochastic variation of microscopic memory	11
3.4. Field dependence of RPM and CPM	12
4. Summary and future prospects	13
Acknowledgments	14
References	14

1. Introduction

A diverse array of systems, including shape-memory alloys, protein molecules and magnetic materials, exhibit memory despite having a multitude of microscopic, strongly interacting degrees of freedom. The necessarily non-ergodic processes that produce memory in soft, hard and biological material systems represent an intriguing aspect of emergent complexity and motivate developing new experimental probes of memory on varying length scales [1, 2]. To what extent does memory in a macroscopic property imply or require memory of microscopic configuration? How does memory evolve as a function of length scale and temperature, in a system with imperfect microscopic memory but perfect macroscopic memory? Under what circumstances can imperfect microscopic memory be quantified with a single-valued function of macroscopic system variables? Surprisingly, simple questions like these have not been extensively studied and the answers remain largely unknown.

Magnetic films offer robust model systems to address these questions, and conversely, these questions are also of significant technological relevance in magnetic recording technologies. For example, by suitably tailoring the structure and surface morphology of a magnetic film it is possible to obtain the desired memory effects. Memory studies also provide an important parameter for characterizing reliable recording material. Previous soft x-ray speckle metrology experiments of Co/Pt multilayer films having perpendicular anisotropy studied return point memory (RPM) and complementary point memory (CPM), which probe the degree to which the magnetic domain structure is reproduced following a full or half magnetization cycle, respectively [3]–[5]. It was found that although the macroscopic magnetization loop showed complete memory, the microscopic RPM and CPM are strongly influenced by sample perfection, disorder and interfacial roughness. The RPM and CPM were found to increase with samples that have higher degree of disorder. More recently, we showed that RPM and CPM can be controlled in exchange-biased [6] antiferromagnetic (AF)–ferromagnetic (F) IrMn–Co/Pt heterostructures by varying the sample cooling conditions to produce a well-defined template in the antiferromagnetic layer [7, 8]. The presence of strong exchange coupling between the F and AF layers results in imprinting a domain template into the AF layer that gives rise to memory effects in the F layer on the mesoscopic length scale. The detailed cause and effect of memory properties in different kinds of magnetic samples vary significantly and have a profound influence on the overall magnetic behavior of the material.

In this paper, we report new coherent soft x-ray speckle metrology studies of RPM in a Co/Pd multilayer film that also exhibits perpendicular anisotropy. We find that in this system the reversal is characterized by domain formation that exhibits nearly a factor of two variation in domain periodicity between initial reversal and magnetic saturation. This is much larger than that exhibited by the Co/Pt films measured previously. This variation, particularly through the associated field-driven changes in domain topology, should impact the microscopic memory in unpredictable ways. We find that the memory is spatially inhomogeneous, with some regions of the film exhibiting no memory at all, whereas others exhibit moderate memory. Further, in the latter regions, the measured memory at a given field cannot be quantified by a single number, but rather is represented by a distribution of values that reflect some variability in the microscopic path through configuration space adopted by the system as the magnetization reverses.

In the next section, we present details of our experimental soft x-ray metrology procedure. We continue with a description and analysis of our results, and conclude with a discussion of how these new results compare to previous results on Co/Pt and some suggestions for further study.

2. Experimental procedures

The Co/Pd multilayer films were prepared by magnetron sputtering on smooth, low-stress 200 nm thick \times 0.5 mm square silicon nitride membranes. The structure of the multilayer is (Ta(2 nm)/Pd(3 nm)/[Co(0.5 nm)/Pd(0.7 nm)]₅₀/Ta(2 nm). The films were grown at room temperature with an 8 mTorr Ar sputtering pressure, leading to moderately rough films [4]. The M versus H hysteresis loop measured by the magneto-optic Kerr effect is shown in figure 1(a). The large Co/Pd interfacial anisotropy leads to perpendicular magnetic anisotropy of the film with a hysteresis loop exhibiting an abrupt domain embryo formation event followed by slower domain enlargement and propagation.

Experiments were performed on beamline 12.0.2.2 at the Advanced Light Source at the Lawrence Berkeley National Laboratory, using an apparatus and procedures described previously [9]. The soft x-ray wavelength was tuned to the Co L_3 absorption edge at 778 eV to achieve magnetic contrast (figure 1(b)) [10]–[15]. The beam exiting the monochromator was focused with Kirkpatrick–Baez optics onto a 10 μ m diameter pinhole to improve the spatial coherence. The experiment was performed in transmission geometry whereby the x-ray beam hits the Co/Pd sample at normal incidence and the scattering pattern was recorded on a CCD camera placed 0.613 m downstream of the sample. An example of the resulting scattering pattern at $H = 192$ mT is offered in figure 1(c). This image, which has had a charge scattering background subtracted as explained in section 3.2, was collected near the coercive field, and shows three primary components [3]–[5], [7, 11]. Near the middle is the shadow of our beam blocker, which protects the camera from the intense unscattered beam and the lower order diffraction fringes from the spatial filter pinhole. Outside the blocker is a ring of diffusely scattered light, the structure of which is determined by the average structure of the labyrinthine domain pattern. Finally, the ring of diffuse light is modulated by ‘speckle’, which is characteristic of the specific illuminated domain pattern. We focus primarily on the speckle component in this paper, since it provides an ‘exact fingerprint’ of the domain structure and can therefore be used to probe domain memory. Such patterns exhibit a speckle contrast of $\sim 50\%$ and could be accumulated with adequate statistics using typically 0.2 s exposures.

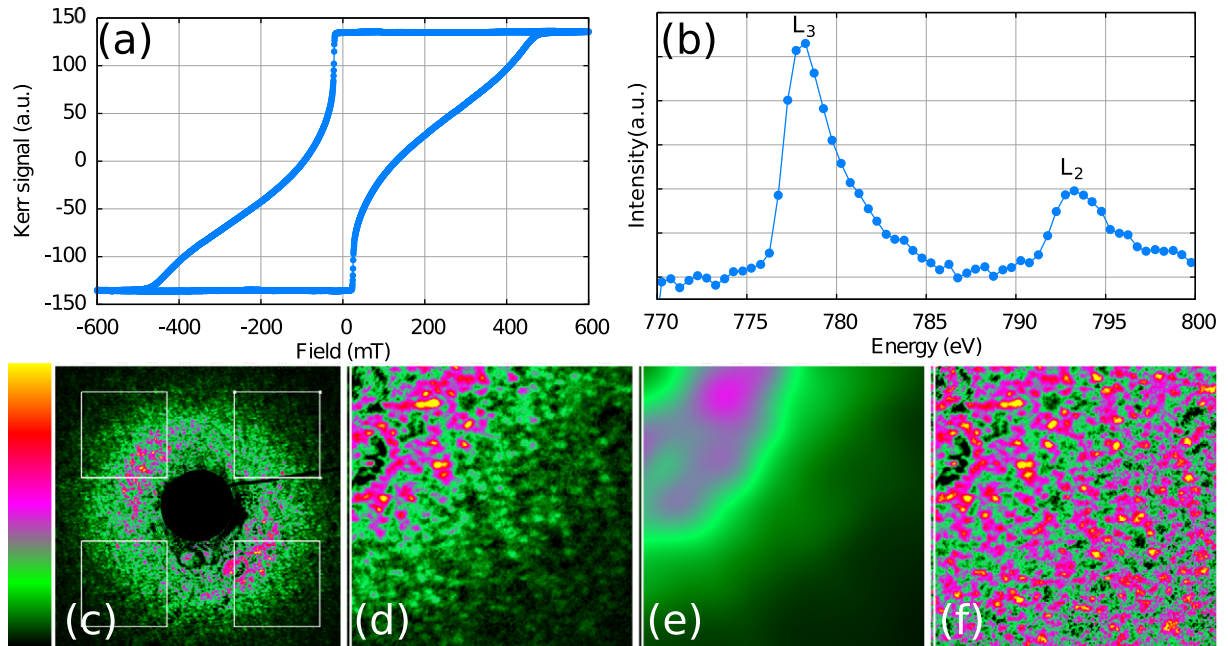


Figure 1. (a) M versus H Kerr magnetization loop for the Co/Pd film. (b) Resonant x-ray absorption scan through the Co L_3 and L_2 edge; all speckle patterns were collected at the peak of the L_2 scattering resonance $h\nu = 778$ eV. Panel (c) shows the background-subtracted speckle pattern at 192 mT, with the four regions of interest used to calculate the speckle correlation functions. The boxes sample nominally the same range of scattering wave vector. The image in (d) is the sub-image in the bottom right of figure 1(c), showing the details in the speckle. A convolution with a 2D Gaussian function of FWHM 30 pixels is shown in (e). The ratio of (d) and (e) is shown in (f), which shows the speckle fingerprint with a constant average of 1.0; this ratio image is used to calculate correlation functions.

In our RPM measurements, we acquired images with the following sequence of applied magnetic fields: $H_A = -510$ mT, $H_B = +H$, $H_C = +H$, $H_D = +510$ mT, $H_E = -H$, $H_F = -H$, $H_G = -510$ mT, repeated four times. This sequence was then repeated at several field values H so as to probe the field dependence of microscopic memory. Comparing images at H_B and $H_E = -H_B$, for example, would provide a single measurement of CPM, whereas comparing pairs of images at H_B is a measurement of RPM. All fields were applied perpendicular to the film and the film temperature in these measurements was 300 K. A field of 510 mT is adequate to saturate the sample magnetization, providing a reference starting point for RPM/CPM measurements. As explained further below, the repeating of $+H$ and $-H$ fields offers a useful calibration and normalization, since the magnetic domains at this temperature and at constant field are static, so sequential images exhibit full ‘microscopic memory’ (i.e. the speckle patterns are perfectly correlated).

3. Results and discussion

3.1. Scattering envelope and average domain structure

The ring of diffusely scattered light evolves with applied field and provides a measure of the average domain width and the degree to which the domains are spatially correlated in the static labyrinth structure. The movie (available from stacks.iop.org/NJP/12/035009/mmedia) shows this evolution graphically. The images in the movie were collected without a spatial filter pinhole in place (the x-ray beam is thus partially coherent), so the speckle contrast is low (7–8%) and the average scattering envelope dominates. At low field, near initial reversal in the magnetization loop, the ring is close to the blocker, corresponding to large domain spacing. As the field magnitude is increased toward the coercive field $H_c = 95$ mT the ring diameter grows significantly, indicating that the average domain period gets smaller. Beyond $H = 380$ mT the ring again decreases in diameter as saturation is approached. The width of the ring, which measures the length scale over which the domains are correlated in space, also first decreases and then increases over this same range of applied field.

We have quantified this behavior by azimuthally averaging the images in the movie to yield scattered intensity as a function of scattering wave vector $I(q)$; this process is analogous to that followed in reducing small-angle x-ray scattering data. These integrated scattering profiles are shown in figure 2(a), and the evolution of the intensity distribution from low to high q as the field is increased is readily apparent. We find that these profiles can be very well fitted to a single Lorentzian with no background, as indicated by the smooth curves in figure 2(a). Figure 2(b) shows the Lorentzian amplitude, center position and width as a function of the applied field. The Lorentzian amplitude is low near initial reversal, maximizes at about twice the coercive field and then vanishes at saturation.

The center position of the scattered intensity as determined by the Lorentzian fit first increases by nearly a factor of two between initial reversal and the maximum at $H = 380$ mT, and then decreases again as saturation is approached. This q -space variation reflects a similar factor of two variation in the average periodicity of the magnetic domains. This variation is much larger than was observed previously in Co/Pt films, where the domain periodicity varied by typically 10% [3]–[5], [11]. One way the large variation in domain periodicity observed in Co/Pd might occur is that, after initial reversal, there is a preferred width for individual reversed domains. These domains form a labyrinth, and the magnetization requires that the average periodicity will necessarily be fairly large near initial reversal. As the field is increased toward the coercive field, more reversed domains of the same preferred width are formed, or more likely the existing domains grow in length and/or the degree of branching. The reduced magnetization then requires a shorter average domain period, as observed. This process is approximately reversed as the sample approaches saturation, with last few domains to switch having a preferred width about the same as the first few to reverse.

The Lorentzian width also shows interesting behavior through the reversal process. The inverse of this width, or the correlation length of the labyrinth, is small near initial reversal and saturation where the domain spacing is large. The Lorentzian center position divided by the Lorentzian width is proportional to the average number of domains having spatially correlated positions. This quantity becomes quite small near initial reversal and saturation but grows monotonically through H_c and beyond, suggesting that the labyrinth is most well formed even beyond the coercive field. The behavior of the Lorentzian width is broadly consistent with the simple model for the reversal process discussed above.

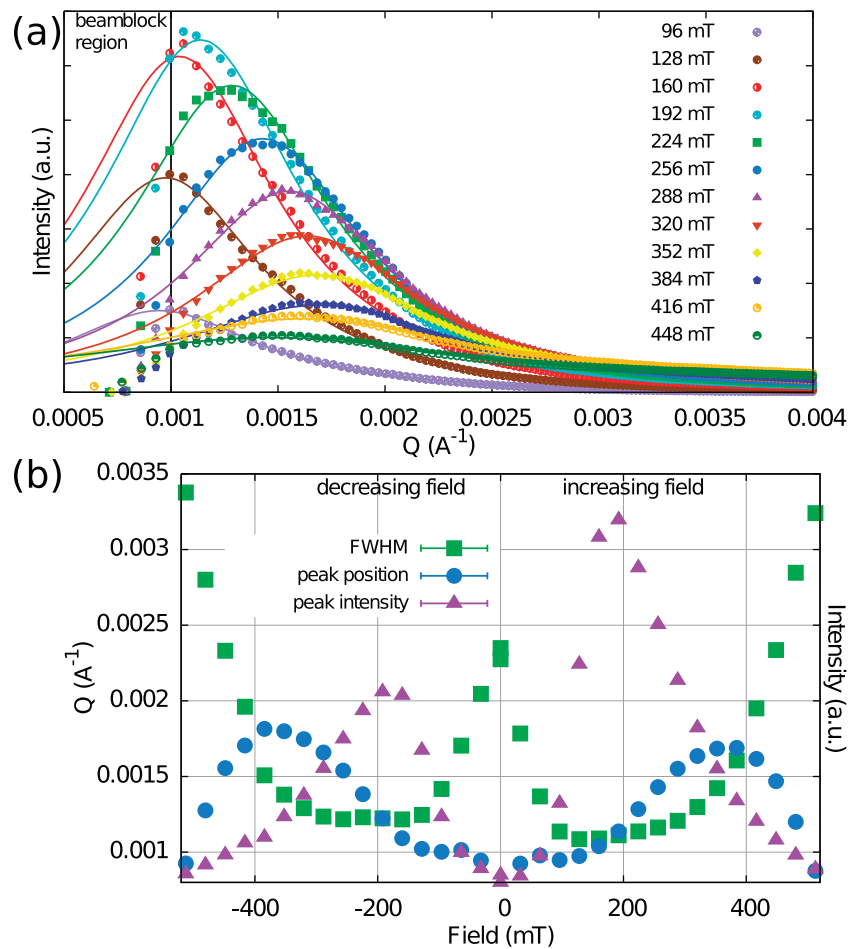


Figure 2. (a) Plot of the radially averaged intensity as a function of scattering vector q for a half-cycle of the hysteresis loop. Shown here are the intensity plots for the lower half (increasing field from negative saturation to positive saturation) of the loop. Solid lines are fits to a single Lorentzian function. The fitting region is defined by the vertical line at $q = 0.001 \text{\AA}^{-1}$, which is the approximate location of the edge of the beam blocker. Panel (b) plots the fitted Lorentzian FWHM (squares), peak position (circles), peak intensity (triangles) of the scattering pattern versus field for both halves of the loop. The right side ($H > 0$) shows the case for field direction of negative saturation to positive saturation, and the left side ($H < 0$) shows the reverse field direction.

Regardless of the precise validity of this simple microscopic model, the reversal process in the current Co/Pd multilayers is notably different from that in Co/Pt multilayers. In the latter, the scattering profiles cannot be fitted with a single Lorentzian with no background. Instead, near initial reversal, a bimodal distribution indicating coexistence of a ‘dilute phase’ of isolated domains and a labyrinthine phase exhibiting spatial correlations between domains qualitatively similar to those between particles in a simple liquid [3]–[5], [11]. In Co/Pd, we do not need to include a dilute phase to model our scattering profiles, and the transition from lower density to higher density labyrinth is continuous and involves a large change in periodicity, at least over the

length scales we can probe. It would be very helpful to probe this system at lower field, where the scattering distribution at present disappears behind our blocker. We return to this issue in the final section.

Finally, it is reasonable to expect that the large variation in domain periodicity with applied field will impact the microscopic memory in a significant way. The labyrinth presents an array of topological centers—branch points, domain ends, etc. The evolution of these centers with field determines part of the microscopic configuration of the domains. Many of the topological magnetic features are also coupled with charge features such as surface roughness, grain boundaries and lattice strain. While preserving these complex interactions, the system needs to reproduce the domain configuration exactly to achieve perfect memory. Yet these topological centers must evolve significantly as the average domain periodicity varies. The much larger evolution in Co/Pd than in Co/Pt suggests that these should exhibit different microscopic memory behaviors.

3.2. Microscopic memory measurements

Our approach is similar to that used in previous studies, although with important differences in detail to improve our accuracy. The first step is to subtract images at saturation from images at field H . The film at saturation has minimal lateral magnetic heterogeneity, so the measured scattering pattern is dominated by charge scattering. In the transmission geometry used here, the charge and magnetic scattered light have orthogonal polarizations and do not interfere, so this subtraction simply removes charge scattering from the images. Slight drift in the apparatus renders the procedure imperfect and, for example, residual pinhole diffraction fringes remain visible near the blocker in the middle of figure 1(c). These fringes cause problems in the microscopic memory measurements, and for this reason we exclude the regions near the blocker in the following analysis.

An RPM or CPM measurement compares two images by cross-correlation to determine the similarity of the speckle fingerprint. Particularly when the signal is low, it is important to subtract different background/saturation images from two images to be cross-correlated. This reduces the impact of Poisson noise in the zero displacement channel of the cross-correlation function (CCF) that is caused by noise in a common background image. This is the reason we adopted the field protocol described in section 2 above. In comparing a CPM pair of images at H_B and H_E , for example, we use background images at H_A and H_D , respectively.

We have developed several approaches to perform the speckle pattern cross-correlations and we describe here the approach that offers the highest accuracy in memory measurements. The background-subtracted images (figure 1(c)) exhibit four components—blocker, average scattering envelope, residual pinhole fringes and speckle fingerprint. Cross-correlating these images directly works, but the resulting CCF images have contributions from all four components. Most problematic are the pinhole fringes, because they exhibit structure on approximately the same scale as the speckle. These are localized near the blocker, and we avoid using this region of the images. We compare four regions in each pair of RPM and CPM images, as indicated by the rectangles in figure 1(c), which avoid significant contamination from the pinhole fringes.

To isolate the speckle features, we divide an average envelope from each image. We find the best way to determine this envelope is to convolve the background-subtracted image with a structure that is larger than a speckle but smaller than other features, e.g. the width of the average

scattering envelope in figure 2(b). Figure 1(e) shows the envelope extracted from the sub-image in figure 1(d) by convoluting with a 2D Gaussian having a 30-pixel full-width half-maximum (FWHM). By comparison, the speckles are < 10 pixels in diameter, and the ring of diffusely scattering light is typically 200 pixels wide. We divide the background-subtracted sub-image by this envelope to produce a ratio image that isolates the speckle fingerprint in figure 1(f). It is apparent from comparing figures 1(d) and (f) that this procedure preserves the speckle fingerprint while nicely flattening the scattering envelope. Note that this convolution causes additional problems near the blocker due to the discontinuity in intensity at the blocker's edge; this is another reason we do not use pixels near the blocker in our analysis. We acknowledge that isolating the speckle from the average envelope, particularly in the presence of partial coherence, is not fundamentally valid [16, 17]. We have done the comparison without isolating the speckle fingerprint, producing the CCF of sub-images like the one in figure 1(d) and then carefully subtracting a CCF 'background' associated with the scattering envelope before integrating the speckle peak. The results are similar to our preferred procedure. We have also varied other non-structural parameters, e.g. the FWHM of the Gaussian used to produce the envelope. Our results are not sensitive to such parameters, so long as the kernel for the convolution is large compared to the size of a speckle and small compared to the width of the ring of diffuse light.

Finally, we form CCF images, using periodic boundary conditions, of each sub-image indicated in figure 1(c) for every RPM and CPM pair of speckle fingerprint images. Figure 3(a) shows a CCF image for an $H_B \times H_C$ pair at $H = 190$ mT, which we refer to as a quasi-autocorrelation image (quasi-ACF). It is a normalized cross-correlation image between two images that are the same, other than Poisson and detector readout noise. When normalized by the number of pixels in the images being correlated, the quasi-ACF image has a flat 'background' with a value of 1.0 and a peak at zero displacement caused by the correlated nature of the speckle. The coherence length of the x-ray beam, the x-ray wavelength and the sample–detector distance collectively determine the width of the speckle peak [16, 17]. The derived value of the transverse coherence length is $\sim 4 \mu\text{m}$, in accord with the expectation based on the optical design of our beamline. The amplitude of speckle peak in this quasi-ACF provides a direct measure of the speckle contrast [16, 17].

A speckle metrology measurement measures the decorrelation of a CPM or RPM pair of sub-images induced by traversing a half or full magnetization cycle, respectively. This decorrelation results in a reduction in the effective contrast measured in a CCF between an RPM or CPM pair. Such a CCF image is shown in figure 3(b) for an $H_B \times H_B$ RPM pair from the same field cycle as in figure 3(a). The speckle peak in this CCF has smaller amplitude than in the quasi-ACF in figure 3(a), and this represents the decorrelation resulting from imperfect microscopic memory. We define a microscopic memory coefficient as

$$\rho(i, j) = \frac{\sum_{\text{speckle}} (\text{CCF}(i, k) - 1)}{\text{sqrt}\left(\sum_{\text{speckle}} (\text{qACF}(i, j) - 1) \sum_{\text{speckle}} (\text{qACF}(k, l) - 1)\right)}, \quad (1)$$

where $\text{CCF}(i, k)$ is the CCF image between ratio sub-images i and k and $\text{qACF}(i, j)$ is similarly the quasi-ACF image between ratio sub-images i and j . As noted above, since these are ratio images with average intensity equal to 1, the 'background' in the correlation images away from the speckle peaks is 1, and this quantity is subtracted from each pixel in the speckle peak before summing. For normalization in the denominator, we use the square root of the two associated quasi-ACFs (e.g. $H_B \times H_C$ and $H_E \times H_F$ for the CCF $H_B \times H_E$); this offers a good normalization

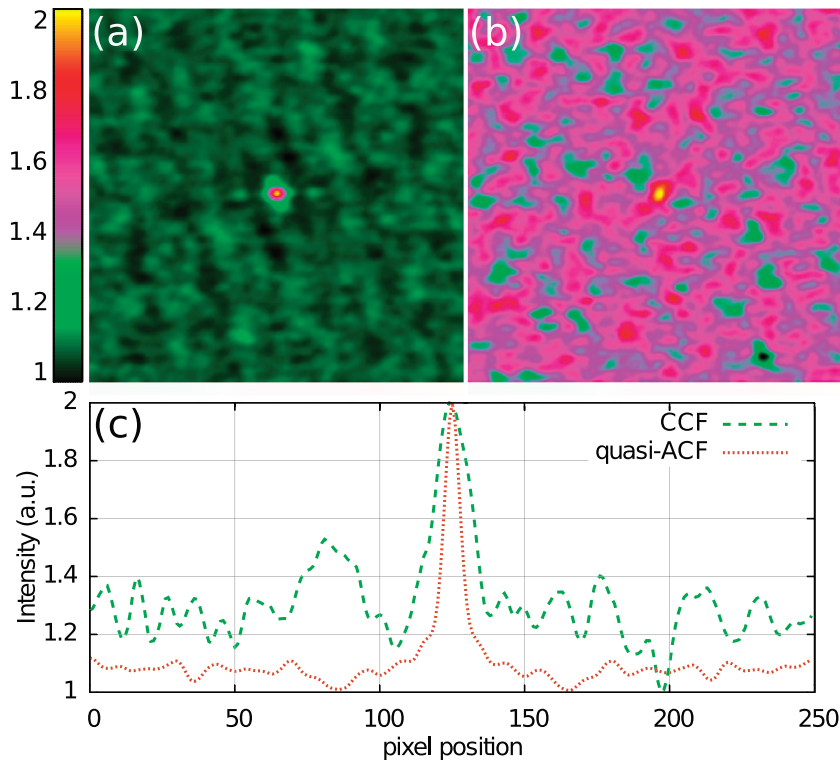


Figure 3. (a) Quasi-ACF and (b) CCF for an RPM pair showing the reduction of the speckle peak amplitude in the latter due to decorrelation of domains through a magnetization cycle. Panel (c) shows the vertical line cuts through the quasi-ACF and CCF speckle peaks, with peaks normalized so that their maxima are the same. In all cases that we have examined closely the CCF speckle peak is notably broader than the quasi-ACF peak. This difference persists if we average speckle peaks produced in many cycles and from all four sub-images in figure 1(c).

for apparatus drift. With this definition, $\rho = 1$ for perfect microscopic memory, whereas $\rho = 0$ for no memory at all. In the RPM pair in figure 3(c), the value of ρ is found to be 0.23. This is the fundamental RPM/CPM measurement we use throughout the rest of this paper.

An assumption in this analysis is that the quasi-ACF and CCF speckle peaks have similar shape and can therefore be compared directly. In our previous studies [3]–[5], [7], Poisson noise impacted the shape of a true ACF used for normalization and made such comparisons difficult, but the use of the quasi-ACF pairs here overcomes this problem. Figure 3(c) shows cuts through the middle of the quasi-ACF and CCF speckle peaks in figures 3(a) and (b). The peak in the CCF has been scaled to have the same amplitude as that in the quasi-ACF. The smaller CCF speckle peak endows this image with larger noise, but more importantly the CCF speckle peak is nearly two times wider than the quasi-ACF peak. As explored in the concluding section, we think this is an important observation since it suggests coupling between neighboring Fourier components in the reversal process. This will be the focus of a future study. In this paper, the summation over pixels in the CCF and quasi-ACF speckle peaks in equation (1) averages over this coupling.

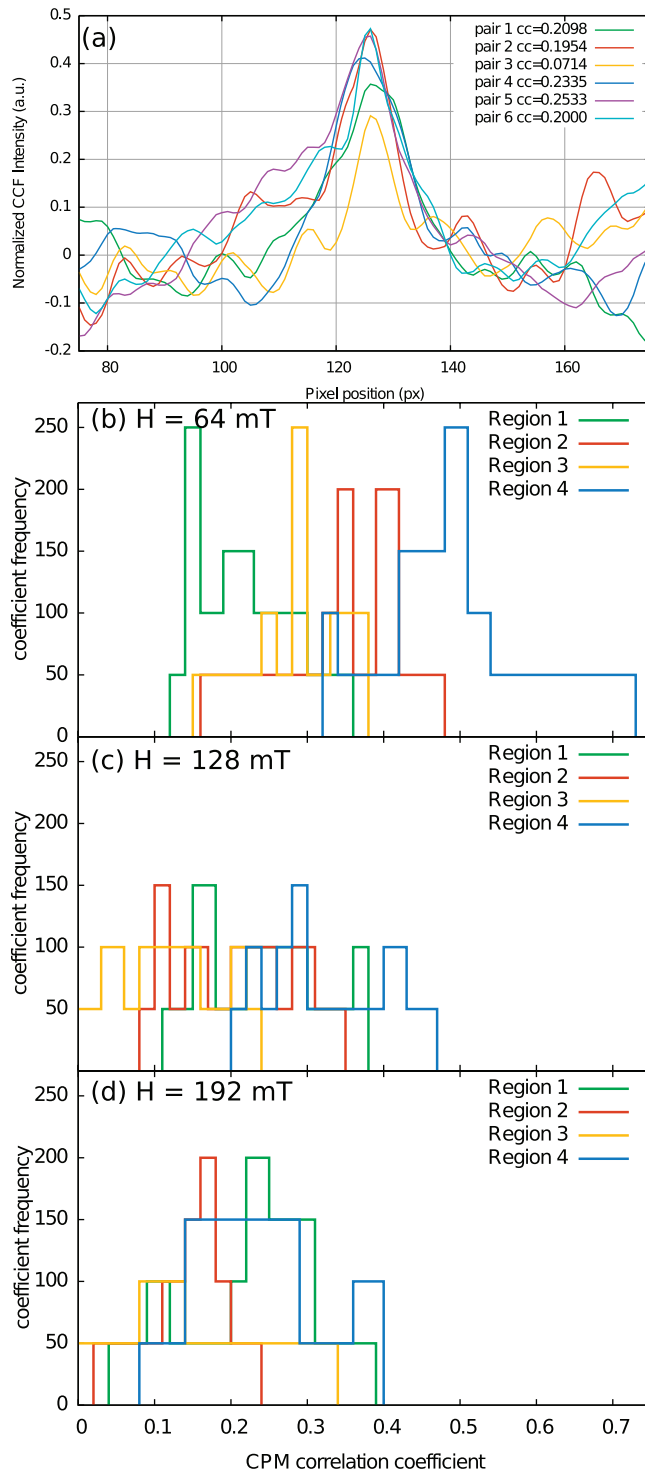


Figure 4. (a) Vertical line cuts through the CCF speckle peaks for six RPM pairs collected at $H = 192$ mT. The line cuts are from region 1, located in the bottom right of figure 1(c). The CCF line cuts are normalized by the area-averaged ACF functions so that they can be directly compared. Panels (b), (c) and (d) are histograms of memory values for all CPM pairs at $H = 64$, 128 and 192 mT, respectively, for the four regions shown in figure 1(c).

3.3. Stochastic variation of microscopic memory

In previous RPM and CPM studies, the measured values have been reported as a single-valued function, that is, $\rho = \rho(H)$, which was measured reproducibly in different magnetization cycles and independent of the position probed on the sample and of the region of the speckle pattern used in the cross-correlation analysis. Imperfect microscopic memory implies variation in the path adopted through a very complex configuration space during reversal, and there really is no reason why all the cycles should yield the same measured memory. Previous measurements supported a single-valued memory function, since repeated measurements produced similar values at the same or at different positions of the sample, at least within the estimated uncertainty of the analysis [3]–[5], [7]. Our improved analysis offers the opportunity to test this conclusion.

Figure 4(a) shows slices through CCF speckle peaks for various RPM pairs at $H = 192$ mT. These have been scaled by their respective quasi-ACF results, and thereby provide a graphic view of a variation of measured RPM in different cycles. Although the images are noisy, the variation is larger than our experimental uncertainty: different cycles do indeed provide slightly different values for microscopic memory. These differences are larger than the variation between RPM and CPM that was reported previously for Co/Pt [3]–[5]. Similar variation is observed when comparing the different regions on the detector in figure 1(c), which probe a similar range of scattering wave vector magnitudes. We collect all CPM measurements in the four rectangular sub-images in figure 1(b) into histograms in figures 4(b)–(d) for $H = 64$, 128 and 192 mT, respectively. Although the limited number of measurements renders these histograms too noisy for a detailed analysis of the distribution, it does point to the fact that rather than a single valued function, the microscopic memory is characterized by a distribution of values. Determining the shape and characteristics of these distributions will be the focus of a future study. In what follows, we report average memory and the standard deviation around this average as a function of field, acknowledging that we cannot determine with accuracy the shapes of the histograms so as to validate precisely these simple statistical measures.

The variation of microscopic memory with position on the sample is even larger than the variation from cycle to cycle discussed above; in some places on the film, the memory is smaller than our ability to measure it. As noted in section 2, the film is grown on a smooth substrate and under conditions where a moderately rough texture should be produced. In our studies of Co/Pt films, a close relationship between film perfection and memory was discovered and discussed in detail [3]–[5], [7]. A Co/Pt film with comparable roughness to the Co/Pd film in this study exhibited similarly imperfect memory, but that memory was reproducibly measured from point to point across the film. In the Co/Pd film, we speculate that there are microscopic stresses that are not uniform and that lead to position-dependent RPM and CPM. Possibly, the differences in average domain behaviors between Co/Pt and Co/Pd discussed in section 3.1 lead to magnetoelastic effects that generate these local stresses. In the present study, these observations indicate that we have not measured a true statistical ensemble of domains. We illuminate a $\sim 10 \mu\text{m}$ diameter spot on the film, and this samples $\sim 10^4$ domains. This is adequate to provide a precise measure of local RPM and CPM, as discussed above. However, if we could perform measurements with a much larger illuminated spot, we would integrate over this sample heterogeneity as well. The RPM and CPM values measured in this case would evidently be smaller than those reported below. Apparently, the Co/Pd film exhibits heterogeneity on a broad range of length scales.

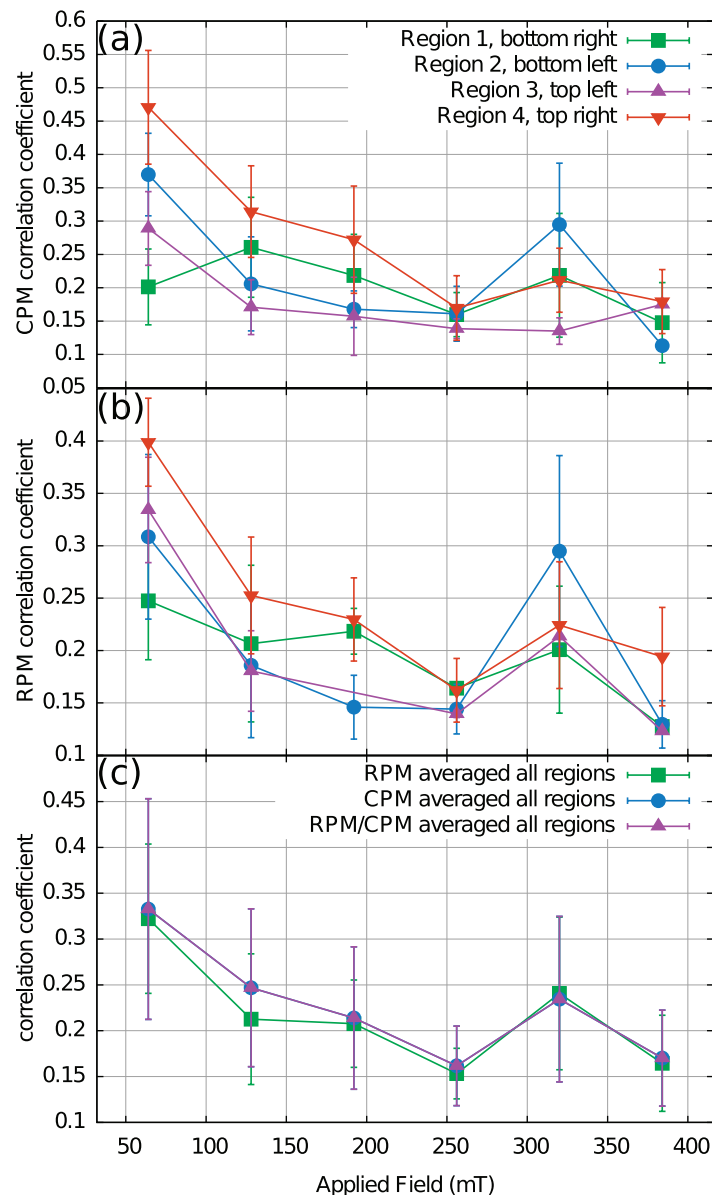


Figure 5. Panels (a) and (b) plot the measured values of the correlation coefficient ρ for CPM and RPM, respectively, as a function of field for the four regions shown in figure 1(c). The error bars reflect the $1 - \sigma$ variation of the memory from cycle to cycle. Panel (c) shows similar RPM and CPM results, averaged over the four regions and over all RPM and CPM pairs.

3.4. Field dependence of RPM and CPM

Figures 5(a) and (b) show the cycle-averaged field dependence of CPM and RPM for the four different sub-images indicated in figure 1(c). The error bars plot standard deviation around these averages associated with the stochastic variation discussed above, and typically amount to 20–30% variation of the measured values. The results for the sub-images generally indicate the same trends, although a more careful examination of the memory values indicates that the variation from sub-image to sub-image in a single RPM or CPM measurement is comparable

to the cycle-to-cycle variation noted above. For this reason, figure 5(c) provides cycle- and sub-image-averaged results for RPM and CPM, again with error bars reflecting the systematic variation of the memory values in terms of the standard deviation. In both cases, the best memory is observed near initial reversal. This was also observed in Co/Pt and reflects the observation that those points on the film that reverse first generally exhibit the best RPM and CPM. Unlike Co/Pt, there is no obvious difference between RPM and CPM, or more accurately, the stochastic variations discussed in section 3.3 are larger than any apparent difference between RPM and CPM. Figure 5(c) also provides the average memory of all cycles, sub-images and RPM and CPM pairs.

4. Summary and future prospects

Few systems, magnetic or otherwise, have been studied from the perspective of microscopic memory. It is therefore prudent to be conservative in drawing broad conclusions at this point. However, the Co/Pt and Co/Pd films are similar enough in properties that one might expect similar behaviors. In this paper, we have shown that they behave differently in at least two ways: (i) the evolution of the average domain periodicity with field and (ii) the variation of microscopic memory from loop to loop and from position to position on the film. Possibly these are related: the stresses associated with variation of a factor of two in domain periodicity likely impacts other magnetic phenomena. Superficially, Co/Pt films with good structural perfection reverse magnetization through a separation between a dense labyrinthine phase and a dilute phase with isolated domains. Over the range we can access, Co/Pd, on the other hand, appears to stay in a single labyrinthine phase of variable periodicity and perfection.

It would be useful to extend our results to lower scattering wave vector so that the average structure of the labyrinthine can be probed closer to the initial reversal. We could then test the above statement about the lack of phase separation in Co/Pd more precisely. The primary limitation in this regard is the hard edges on our spatial filter pinhole. These produce Airy fringes that decay algebraically and so extend into the diffuse scattering regime. As are other research groups around the world, we are working on producing pinholes with soft edges so as to reduce the intensity and extent of the resulting fringes.

Understanding the subtle features of microscopic memory will likely also benefit from measuring the temperature dependence of our results. The domains in our film are essentially static at constant field, meaning that the film temperature does not strongly impact the equilibrium film properties. However, magnetic reversal involves traversing a complex energy landscape, where small thermally induced variations in path can lead to loss of microscopic memory. Can we reduce these variations, and thereby improve the microscopic memory, by cooling the films? Alternatively, will the distribution of RPM and CPM measurements change at lower temperature? Will the shape of the CCF speckle peak depend on temperature? It seems that differences in the shape of ACF and CCF speckle peaks might be a common feature in complex systems, and microscopic memory offers an interesting way to probe this complexity.

Related to the temperature dependence will be the ability to resolve the dependence of microscopic memory on the scattering wave vector q so that different length scales can be probed. Very likely a q -dependence at large q will be coupled to a T -dependence because variation in domain reversal and boundaries will play a larger role at shorter length scales. Such studies will also allow us to observe the transition between imperfect microscopic memory and perfect macroscopic memory of the magnetization loop; again, accessing smaller q with a soft pinhole would be very helpful in this regard.

Finally, we wish to mention the broader importance of applying coherent x-ray beams to probe microscopic memory in nanostructured material systems. The phenomenon has been studied very little, yet in many nanoscale systems memory effects might be important since the impact of defects and imperfections becomes correspondingly higher. These are difficult to control, but they can determine switching and, therefore, the memory of many logic operations. Magnetic films provide nice model systems to study these phenomena. Memory effects also offer an excellent example of why it is important to probe nanostructured systems statistically jointly in q -space with scattering and in real space with microscopy. The RPM we measure results from a multitude of events—Barkhausen cascades—that either force a system to follow a particular path (the non-ergodic result) or allow the flexibility to decorrelate and to lose memory. It is important to probe average properties and to compare these to specific microscopic events. This paper and previous papers [3]–[5], [7] show how coherent soft and hard x-ray speckle metrology techniques offer robust statistical probes of microscopic memory; other papers in this volume describe progress in the field of x-ray diffractive imaging, which will eventually allow us to illuminate the relationship between detailed microscopic events and statistical averages.

Acknowledgments

This work was supported in part by the National Science Foundation under grant number DMR-0506241. This work at ALS/LBNL was supported by the Director, Office of Science, Office of Basic Energy Sciences, of the US Department of Energy under contract no. DE-AC02-05CH11231.

References

- [1] Laughlin R B 2005 *A Different Universe: Reinventing Physics from the Bottom Down* (New York: Basic Books)
- [2] Laughlin R B, Pines D, Schmalian J, Stojković B P and Wolynes P 2000 The middle way *Proc. Natl Acad. Sci. USA* **97** 32
- [3] Pierce M S *et al* 2007 Disorder induced magnetic memory: experiments and theories *Phys. Rev. B* **75** 144406
- [4] Pierce M S *et al* 2005 Disorder-induced magnetic memory *Phys. Rev. Lett.* **94** 017272
- [5] Pierce M S, Moore R G, Sorensen L B, Kevan S D, Hellwig O, Fullerton E E and Kortright J B 2003 Quasistatic x-ray speckle metrology of microscopic magnetic return-point memory *Phys. Rev. Lett.* **90** 175502
- [6] Nogués J and Schuller I K 1999 Exchange bias *J. Magn. Magn. Mater.* **192** 203
- [7] Chesnel K, Fullerton E E, Carey M J, Kortright J B and Kevan S D 2008 Magnetic memory in ferromagnetic thin films via exchange coupling *Phys. Rev. B* **78** 132409
- [8] Kappenberger P, Martin S, Pellmont Y, Hug H J, Kortright J B, Hellwig O and Fullerton E E 2003 Direct imaging and determination of the uncompensated spin density in exchange-biased CoO/(CoPt) multilayers *Phys. Rev. Lett.* **91** 267202
- [9] Chesnel K, Turner J J, Pfeifer M and Kevan S D 2008 Probing complex materials with coherent soft x-rays *Appl. Phys. A* **93** 431
- [10] Dudzik E, Dhesi S S, Durr H A, Collins S P, Roper M D, van der Laan G, Chesnel K, Belakhovsky M, Marty A and Samson Y 2000 Influence of perpendicular magnetic anisotropy on closure domains studied with x-ray resonant magnetic scattering *Phys. Rev. B* **62** 5779
- [11] Hu B, Geissbuhler P, Sorensen L, Kevan S D, Kortright J B and Fullerton E E 2001 Coherent soft x-ray magnetic scattering *Synch. Rad. News* **14** 11

- [12] Kortright J B, Awschalom D D, Stohr J, Bader S D, Idzerda Y U, Parkin S S P, Schuller I K and Siegmann H-C 1999 Research frontiers in magnetic materials at soft x-ray synchrotron radiation facilities *J. Magn. Magn. Mater.* **207** 7
- [13] Kortright J B, Hellwig O, Marguiles D T and Fullerton E E 2002 Resolving magnetic and chemical correlations in CoPtCr films using soft x-ray resonant scattering *J. Magn. Magn. Mater.* **240** 325
- [14] Kortright J B, Jiang J S, Bader S D, Hellwig O, Marguiles D T and Fullerton E E 2003 Magnetism in heterogeneous thin film systems: resonant x-ray scattering studies *Nucl. Instrum. Methods B* **199** 310
- [15] Kortright J B, Kim S-K, Denbeaux G P, Zeltzer G, Takano K and Fullerton E E 2001 Soft-x-ray small-angle scattering as a sensitive probe of magnetic and charge heterogeneity *Phys. Rev. B* **64** 1
- [16] Dainty J C 1975 *Laser Speckle and Related Phenomena* (Berlin: Springer)
- [17] Goodman J 1985 *Statistical Optics* (New York: Wiley)